Journal of Coastal Research	12	4	984–995	Fort Lauderdale, Florida	Fall 1996

Remote Sensing of Turbid Coastal and Estuarine Waters: A Method of Multispectral Water-Type Analysis

Oscar Karl Huh†, Christopher C. Moeller‡, W. Paul Menzel‡, Lawrence J. Rouse, Jr.†, and Harry H. Roberts†

†Coastal Studies Institute
Louisiana State University
Baton Rouge, LA 70803,
U.S.A.

‡Cooperative Institute for
Meteorological Satellite
Studies
University of Wisconsin–
Madison
1225 West Dayton Street
Madison, WI 53706, U.S.A.

ABSTRACT

HUH, O.K.; MOELLER, C.C.; MENZEL, W.P.; ROUSE, L.J., Jr., and ROBERTS, H.H., 1997. Remote Sensing of Turbid Coastal and Estuarine Waters: A Method of Multispectral Water-Type Analysis. *Journal of Coastal Research*, 12(4), 984–995. Fort Lauderdale (Florida), ISSN 0749-0208.

Analysis of digital imagery from the 100 m resolution airborne Multispectral Atmospheric Mapping Sensor (MAMS) indicates that scatter plots of remotely sensed sea surface temperature versus visible and near infrared subsurface reflectance can be used to quantitatively distinguish coastal water types. The Louisiana Gulf coast, a complex region of deltas, estuaries, and marshy wetlands, is the setting for this work. Gulf inner shelf and Mississippi River waters are the primary source water types, but four additional water types are formed locally and are readily detectable with MAMS including: shallow ambient bay water, fresh marsh water drainage, salt marsh drainage, and soil water drainage. *In situ* measurements of suspended sediment concentration and sea surface temperature in the Atchafalaya and adjacent bays have verified the characteristics of these water types. It is found that under the forcing of atmospheric cold front passages, water type differentiation is enhanced, creating a mosaic of water types in these coastal waters. Multispectral remote sensing of these complex, variably turbid coastal waters, provides data useful for studies of water type formation and coastal circulation processes.

ADDITIONAL INDEX WORDS: *Atmospheric cold fronts, suspended sediments, coastal circulation, Multispectral Atmospheric Mapping System, SPOT images, atmospheric correction, Aircraft multispectral scanner, Chenier Plain, Atchafalaya Bay, Atchafalaya River.*

INTRODUCTION

Mapping the presence, distribution, and boundaries of various water types is important to a number of problems common to coastal regions around the world. In these environments of complex, time dependant air-sea-river-land interactions, coastal circulation is the essential variable. It is the primary control on physical properties, affecting the fate of toxic pollutants, the movement of fish larvae, the location of fish schools and other marine life, as well as location of erosion and sedimentation sites. The dynamics of coastal and estuarine fronts bounding the water types tend to concentrate water borne pollutants (KLEMAS, 1980).

From space and airborne optical imagery, impressive comprehensive views of coastal waters have been obtained for many years. Aircraft and manned spacecraft photography, and Landsat imagery for example, have provided intriguing color imagery of coastal waters. The coastal region often appears as a patchwork of plumes, mud streams, and zones of various colors and transparencies, distributed from river mouths and surf zones to as far away as the continental shelf edge. However, for most applications, qualitative depiction of color variations is of very limited use. In situ oceanographic analysis traditionally measures temperature and salinity as parameters of primary importance. Without remote salinity sensing systems at appropriate spatial resolution in the near future, water temperature and turbidity/reflectance measurements provide the useful parameters from airborne and spaceborne sensors.

The purpose of this paper is to demonstrate that moderate spatial resolution (100 m or better) multispectral remote sensing of surface temperature and turbidity can quantitatively discriminate water types in complex coastal regions with high levels of sediment loading. The Multispectral Atmospheric Mapping Sensor (MAMS), a multispectral imager that flies on board NASA's ER-2 research aircraft, provides visible, near infrared and infrared thermal imagery at 100 m resolution. This study is an analysis of MAMS data and how it depicts variability of coastal waters. The System Probetoire pour Observatione de la Terre (SPOT), a spaceborne multispectral imager, also provides useful high resolution (20 m) visible/near infrared imagery. While the SPOT data are useful for many inshore studies, the need for a thermal channel restricts it's utility here.

This study is focused on the Atchafalaya-Chenier Plain sedimentary system (HUH *et al.*, 1991) shown in Figure 1. The Atchafalaya River brings 152 km^3 of turbid fresh water

95028 received 10 March 1995; accepted in revision 10 October 1995.

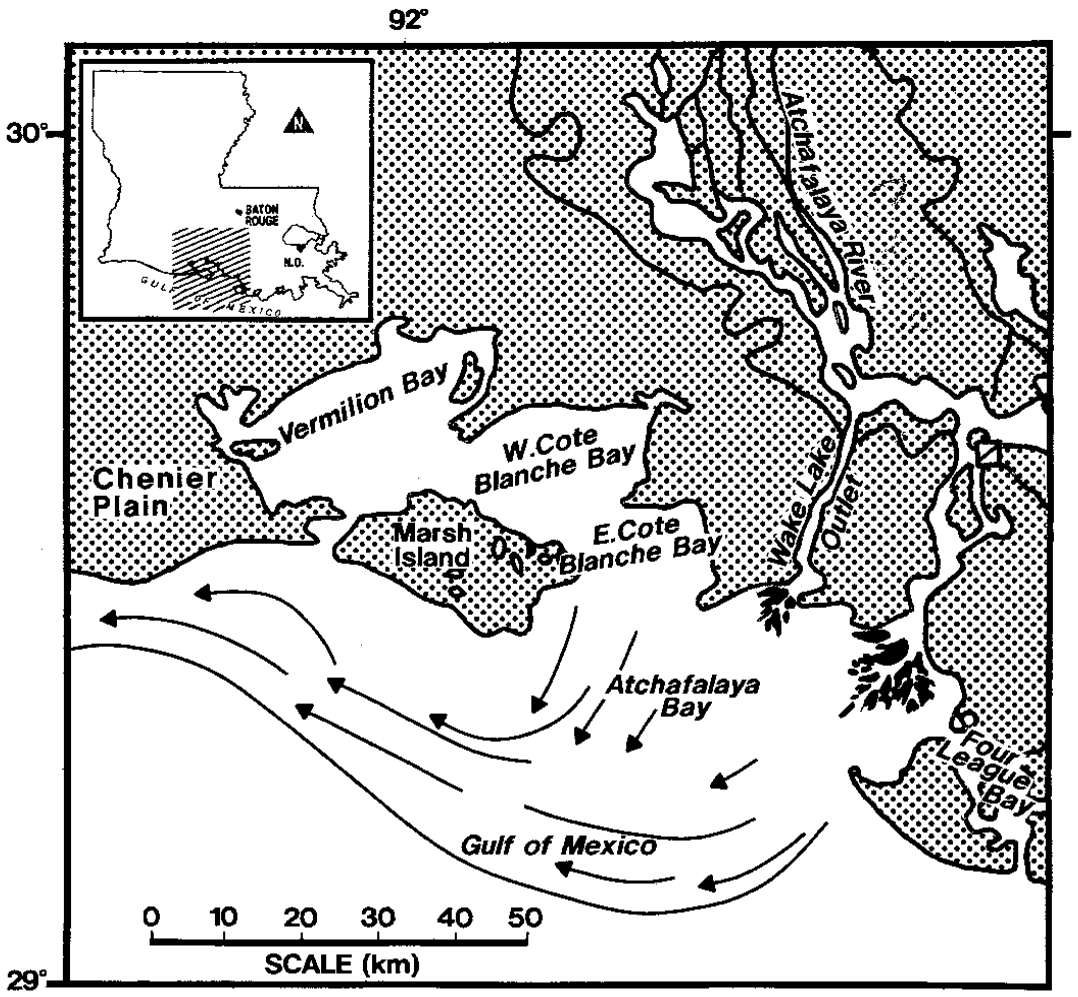

Figure 1. Location map of the study area. The arrows indicate the prevailing transport of surface water and suspended sediment.

(WALKER and ROUSE, 1993) and 88 × 10^6 tons of sediment (ROBERTS and VAN HEERDEN, 1992) into coastal and Gulf of Mexico waters annually (WALKER and ROUSE, 1993). In this deltaic coastal zone, these waters meet in a complex of environments including fresh water marshes, salt water marshes, estuaries, bays, tidal flats, river mouths, deltas and inner continental shelf (Figure 1). Suspended sediment concentrations range up to 1200 mg/l. and more. This coastal region has a broad (100–200 km), shallow continental shelf, is strongly influenced by river runoff, is microtidal (< 1m, semidiurnal), and is experiencing active subsidence (tectonic-compactional-fluid withdrawal) of 1.65 cm/yr. (PENLAND and RAMSEY, 1990). It will be shown that within this complex of environments, atmospherically driven processes alter the physical properties and seston content of local marine and river waters to generate additional water types.

MULTISPECTRAL REMOTE SENSING SYSTEMS, MAMS AND SPOT

A series of 2–4 hour NASA ER-2 aircraft missions have been flown over coastal Louisiana acquiring MAMS imagery and color aerial photography. The MAMS is a cross track, line-scanning, multispectral radiometer (JEDLOVEC *et al.*, 1989; MOELLER *et al.*, 1989). At the operational altitude of 20 km the 5 milliradian aperture yields 100 m resolution at nadir in 12 visible/infrared channels (Table 1). The swath width is 37 km. Calibration of the infrared channels is accomplished by viewing two on-board blackbodies of known temperature during each scan. Visible and near infrared calibration is measured optically in the laboratory before and after MAMS deployments through the use of an integrating sphere at Ames Research Center, California. Voltage output from each MAMS radiation detector is recorded digitally (8 bit precision) on board the aircraft and converted to geophysical units dynamically in the laboratory. A dynamic calibration software package (JEDLOVEC *et al.*, 1989) on the Man-computer-Interactive-Data-Access-System (McIDAS, SUOMI *et al.*, 1983) at the University of Wisconsin converts raw digital counts to radiances for the visible and near infrared channels (channels 2–8) and to radiances and blackbody equivalent temperatures for the thermal channels (channels 9–12). Earth location and rectification of the imagery is accomplished using McIDAS navigation software in conjunction

elling studies, GORDON (1978), and GORDON *et al.*, (1983), developed a single scattering atmospheric correction method. The total radiance, L, arriving at the sensor is expressed as the sum of molecular scattering (L_r), aerosol scattering (L_a), sun glint (L_g), and the water leaving radiance (L_w) diffusely transmitted by the atmosphere.

$$L = L_r + L_a + L_g + tL_w$$

The diffuse transmittance t is used rather than the direct transmittance to account for the sensor receiving photons from regions adjacent to the field of view under examination.

Molecular scattered path radiance L_r and aerosol scattered path radiance L_a are expressed as the sum of photons scattered in the atmosphere directly into the sensor, and photons scattered in the atmosphere and then reflected back by the surface into the sensor. Expressions for molecular scattering optical depth and ozone optical depth (absorption) are given by GUZZI *et al.* (1987). Aerosol optical depth was estimated using relationships between surface visibility and aerosol optical depth given by Sturm (1981). Sun glint radiance L_g was estimated using sun-sensor geometry and surface wind speed data in a model by GUZZI *et al.* (1987).

After atmospheric effects have been removed, the remaining water leaving radiance is expressed as a subsurface reflectance according to ROBINSON (1985). The subsurface reflectance quantity can be regressed against *in situ* suspended sediment concentration (SSC) data; however, *in situ* data were not sufficient to establish reliable SSC regression coefficients for March 30 and April 1, 1989. Therefore, MAMS visible and near infrared reflectance images in this paper are displayed as a scaled subsurface reflectance quantity. Further discussion of the atmospheric correction of MAMS radiances can be found in GUMLEY *et al.* (1990).

Atmospheric Correction of Infrared Data

MAMS 11 μm and 12 μm infrared radiances were used to correct for atmospheric water vapor effects in estimating sea surface temperature (SST). A split window algorithm (MCMILLIN and CROSBY, 1984) was used

$$SST = T_{11} + A(T_{11} - T_{12}) + B$$

where T_{11} and T_{12} are the MAMS 11.2 μm and 12.5 μm brightness temperatures, A is a regression coefficient, and B is a bias correction. Robust values for A and B have not yet been determined for MAMS split window channels; because MAMS split window channels are similar to those of the geostationary VISSR Atmospheric Sounder (VAS), an instrument used previously to estimate SST (see BATES *et al.*, 1987), VAS SST coefficients were used. A bias correction between MAMS and VAS 11 μm and 12 μm radiances was applied to remove absolute calibration differences between the instruments. Tests using MAMS-specific SST coefficients under development showed only minor difference (<1 K) from using the VAS SST coefficients to estimate SST.

CASE STUDY RESULTS

Cold Front Passage of 31 March 1989

In the early spring of 1989, MAMS was deployed to Patrick AFB, Florida, for a series of flights along the Louisiana coast on NASA's ER-2 high altitude aircraft. The objective was to obtain MAMS imagery of coastal conditions during both pre-frontal and post-frontal phases of a cold front passage. This objective is difficult as pre-frontal mid and upper level clouds often obscure the coastline during the cold front season. However, a weak relatively cloud-free synoptic low which had formed in Texas on March 29, strengthened and proceeded with minimal cloudiness through the Louisiana coastal region with frontal passage occurring late on March 30 into early morning of March 31. MAMS was flown on the morning of March 30 twelve hours prior to frontal passage, and on the morning of April 1, about thirty-six hours after frontal passage.

The cold front propagated west to east at a high angle to that of the coastline orientation. Surface conditions created by this system are illustrated in a time series format in Figure 3 from observations made at the National Weather Service (NWS) station in Lake Charles (LCH), Louisiana. The frontal passage is well defined by the increase in surface pressure beginning about 0200 UTC on March 31 (8 pm LST, March 30). Decrease of air temperature behind the front is illustrated by the temperature minima on the days following the frontal passage (about 3–6 K). Dew point temperatures also decrease behind the front. Surface winds show maximum speeds in the 12 hours preceding and just after the frontal passage with a southwest to northerly wind shift. Thus, while MAMS flew in both the pre-frontal and post-frontal phases, it did not overfly the Louisiana coast during peak winds in either phase. Results of the wind forcing during those peak velocity periods

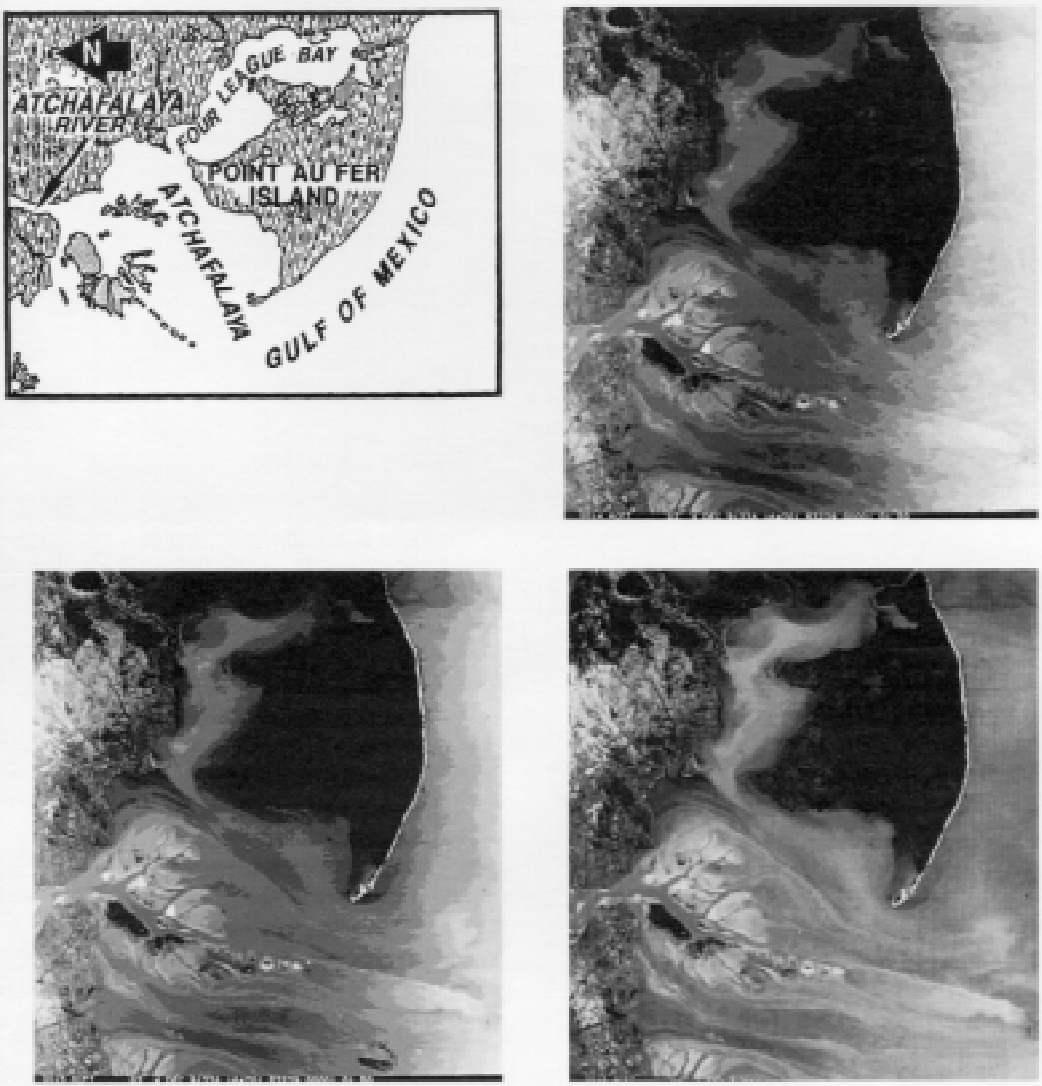

Figure 3. (a) Image location map; (b) MAMS uncorrected band 3 (.56 μm) imagery; (c) after sunglint removal; (d) after atmospheric scattering removal, leaving an image of scaled water leaving reflectance (x = 500-R). Sunglint correction is not attempted over land surfaces.

ATMOSPHERIC CORRECTION

In order to isolate the upwelling radiance from within the water column, atmospheric contributions to total radiance (molecular and aerosol scattering, ozone absorption) in MAMS visible and near infrared channels are removed using a single scattering model (MOELLER *et al.*, 1993; GUMLEY *et al.*, 1990). The contribution by specular reflectance (sunglint) is estimated using principles outlined in Cracknell (1993), by which it is shown that visible sunglint is related to sunglint at thermal infrared wavelengths. In this case, 11 μm sunglint radiance is assumed small compared to the 3.7 μm sunglint radiance. A difference of the 3.7 μm ($T_{3.7}$) and 11 μm (T_{11}) temperatures is taken as representative of the sunglint at 3.7 μm and the visible sunglint, L_{sg}, for channel k is computed by

$$L_{sg,k} = A \cdot (T_{3.7} - T_{11}) + B$$

The coefficients A and B are determined for each visible/near infrared channel using plots of ($T_{3.7} - T_{11}$) versus visible radiance in regions of sunglint, and fine-tuned by the user through close inspection of the sunglint corrected imagery. Effects by atmospheric water vapor absorption and calibration uncertainty, as well as clear water radiance are implicitly accounted for in the value of B. Instrument viewing angle effects on A and B are not explicitly removed, however, the impact appears minimal as no angular biases are evident in the MAMS atmospherically and sunglint corrected imagery (see example in Figure 3). In this figure, cross track variability is evident on the right side of the images 3b and 3c, in the relatively uniform inner shelf waters. Figure 3d shows a "flat" reflectance field offshore as both sunglint and atmospheric scattering effects have been removed. After correcting for sunglint and atmospheric scattering/absorption effects, the resulting water leaving radiance is converted to a subsurface reflectance ratio (water leaving vs incoming radiance). The procedure is outlined in GUMLEY *et al.* (1990). The

Table 2. *Coastal water type analysis albedo in MAMS Band 6 (0.65–0.83 μm, Red-NIP) vs. water surface temperature.*

Water Types	4 DEC Temperature	4 DEC Albedo‡	5 DEC Temperature	5 DEC Albedo‡	Description
Gulf waters					Warm, low turbidity
Mean	17°C	2%	17°C	2%	
St. D.					
Bay waters					Cold, very trubid
Mean	8.54°C	12.6%	6.8°C	10%	
St.D.	0.15°C	0.1%	0.2°C	0.2%	
River waters					Cool, moderately turbid
Mean	11.1°C	9.3%	10.1°C	7.6%	
St.D.	0.03°C	0.2%	0.3°C	0.3%	
Fresh water marsh drainage†					Cool, very low turbidity
Mean	10.2°C	8%	8.5°C	7.2%	
St.D.	0.4°C	0.3%	0.2°C	0.2%	
Salt marsh drainage†					Cool, very low turbidity
Mean	7.9°C	6.5%	6.4°C	7.3%	
St.D.	0.2°C	0.4%	0.2°C	0.7%	
Soil Waters					Very cold in mid-day, very shallow water environments with variable reflectance, possibly caused by subaqueous bottom reflectors
Mean	6.0°C	11.2%	9.3°C	7.8%	
St.D.	1.0°C	0.8%	1.0°C	0.6%	

‡Calculated subsurface reflectance values (R) converted to albedo by 100*R
†Differentiated by location and source

use of a reflectance quantity as opposed to a radiance quantity is desirable because of varying levels of solar irradiance reaching the sea surface, due to changing atmospheric and local solar zenith angle conditions. Multiplying the subsurface reflectance value by 100 converts it into a more conventional albedo value used in Table 2.

MAMS 11 μm and 12 μm data are used to form a split window correction algorithm to remove atmospheric water vapor absorption effects on MAMS thermal infrared data (MOELLER *et al.*, 1993). The resulting sea surface temperature (SST) is not corrected for emissivity effects due to suspended material in the water; the effect of emissivity variation on MAMS 11 μm and 12 μm data over turbid waters can be reasonably expected to be less than 1 K (WEN-YAO *et al.*, 1987).

METHOD OF MULTISPECTRAL WATER TYPE ANALYSIS

The existence of an inverse correlation between MAMS visible/near infrared reflectances and thermal data in coastal waters was first pointed out by MOELLER *et al.* (1989). Digital interactive inspection of the MAMS subsurface reflectance and surface temperature data revealed considerable variability and much useful detail. Greatest discrimination of water variability details are possible in MAMS channel 6 (near infrared) and in water surface temperatures calculated from the MAMS split window channels. Further evidence of the importance of the near infrared part of the spectrum for highly turbid waters can be seen in the comparison of SPOT HRV-1 (0.50–0.59 μm vis.) and HRV-3 (0.79–0.89 μm near IR) data of Atchafalaya Bay (Figures 4a and b). These two images are greatly enhanced but not atmospherically corrected. The faint vertical striping is due to the fact that extra enhancement has revealed the very small differences (1–2 counts) in sensitivity of the Charged Couple Device (CCD) detectors of the "push broom" HRV sensor. Figures 5 and 6 are paired reflectance-temperature MAMS images from 4 and 5 December, 1990, respectively. The images of both days show zones of uniformity with abrupt boundaries between adjacent bodies of water. The flight of 4 December (Figure 5) occured in post-frontal conditions approximately 12 hours after a cold front passage. Surface winds at New Orleans (MSY) Louisiana, were 7.7–10.2 m sec^{-1} from the north. Water levels in the Atchafalaya Bay were very low due to the combined effects of post-frontal water level set down and low astronomical tide. The 5 December flight (Figure 6) occurred some 24 hrs after a slackening of winds. Subsurface reflectance and water surface temperatures were extracted from the labeled polygons in Figures 5 and 6 and plotted in a temperature/reflectance scatter plot (Figure 7). This diagram is analogous to a temperature/salinity plot used for differentiating ocean waters of various origins. The plot quantifies the separability of the water types. Knowledge of the local sediments and hydrology of the Atchafalaya Bay region along with the reflectance and thermal properties in Figures 5 and 6 allow us to label each water type in Figure 7. The six water types identified are summarized in Table 2. Several of these water types (Gulf, Bay, River) have been identified using suspended

→

Figure 4. Contrast stretched SPOT images of the Atchafalaya River Delta and a portion of the surrounding Bay: (a) visible "green" band HRV-1 (0.50–0.59 μm), (b) near infrared band HRV-3 (0.79–0.89 μm). Note the greater detail in the HRV-3 image which has *least* water penetration depth.


Hrv-1

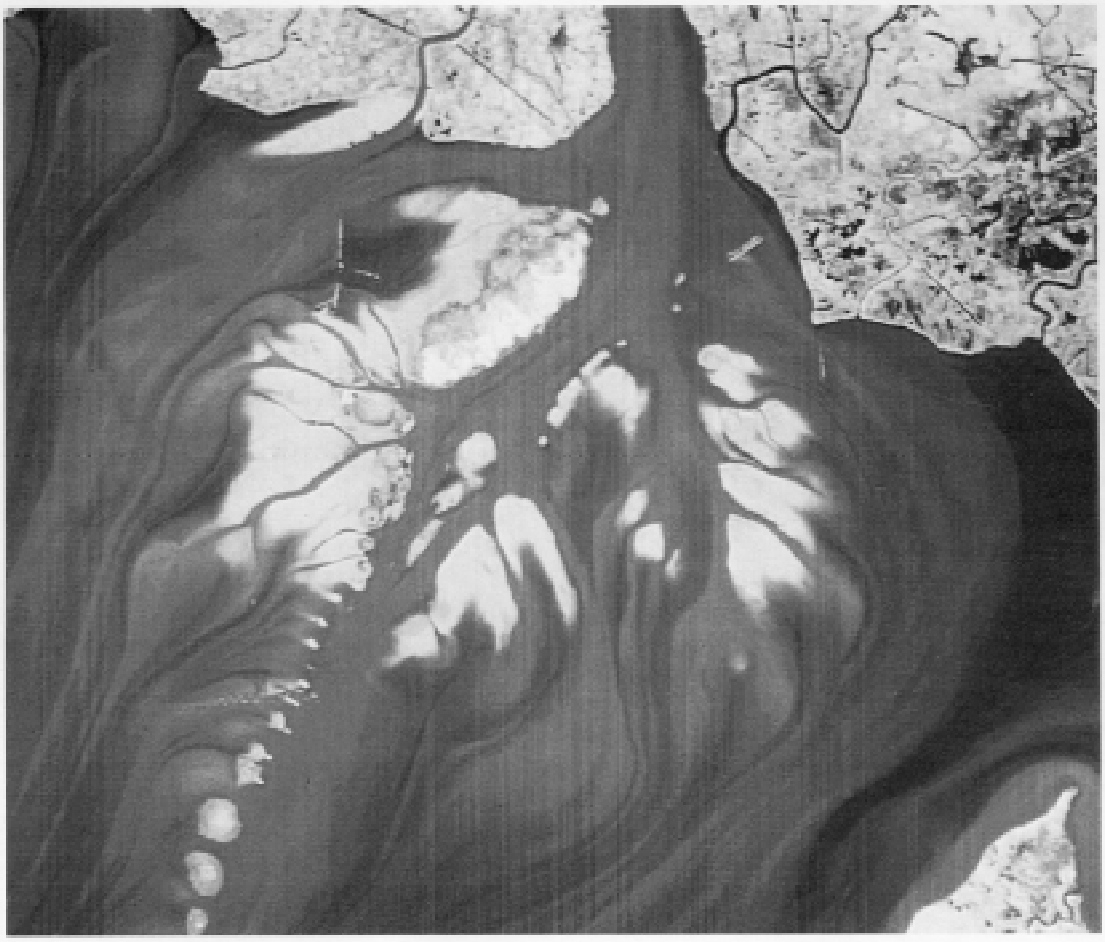

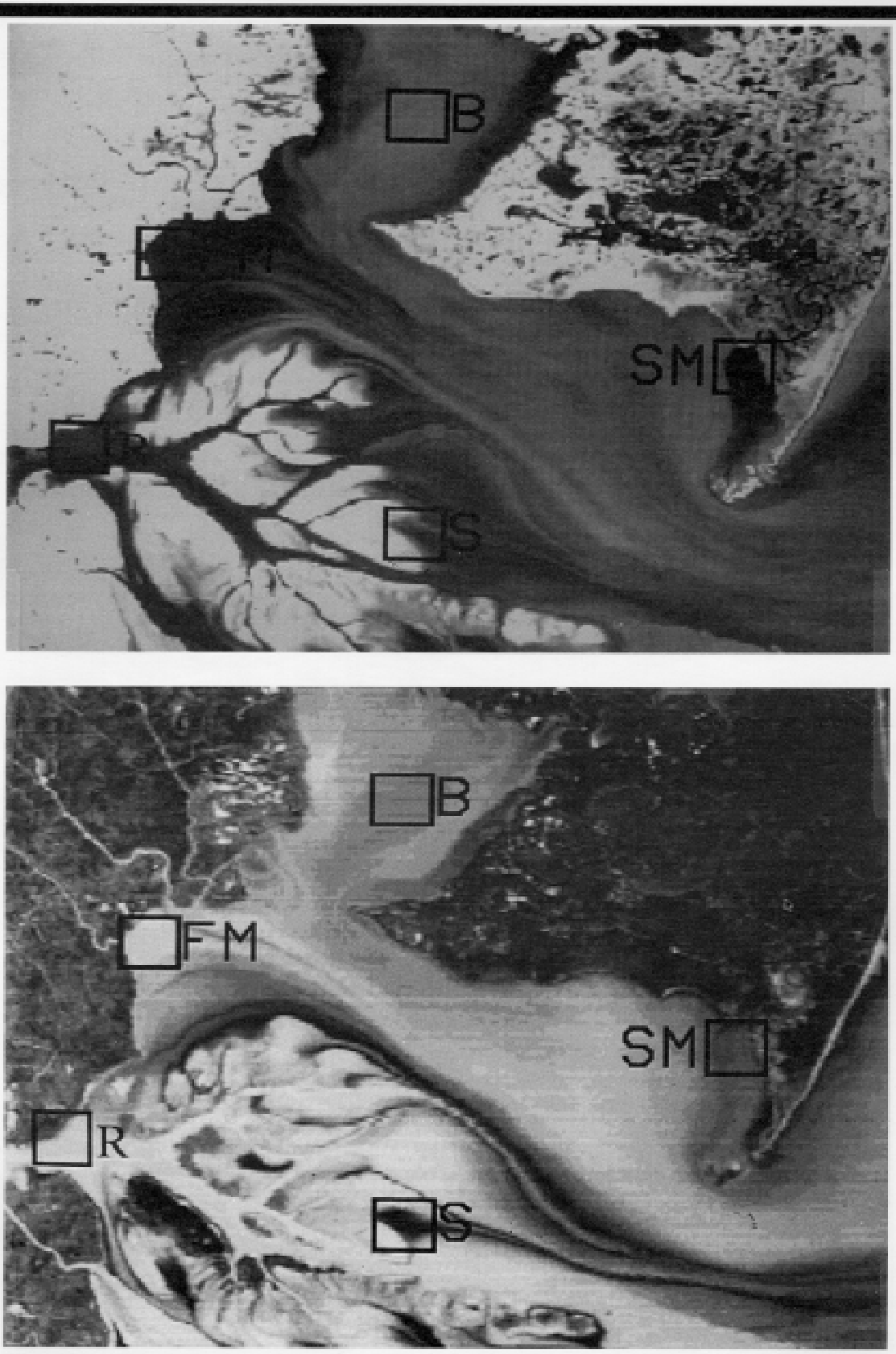

Figure 5. MAMS images of (a) band 6 (0.65–0.83 μm) subsurface reflectance and (b) split window surface temperature for 4 December 1990, approximately 12 hrs after frontal passage. Land reflectance is high (white tones) in the reflectance image. Boxes represent regions of images sampled for 4 December values shown in Figure 7, water types indicated are FM = Fresh Water Marsh; B = Bay water; S = Soil water; SM = Salt Marsh; R = River water.

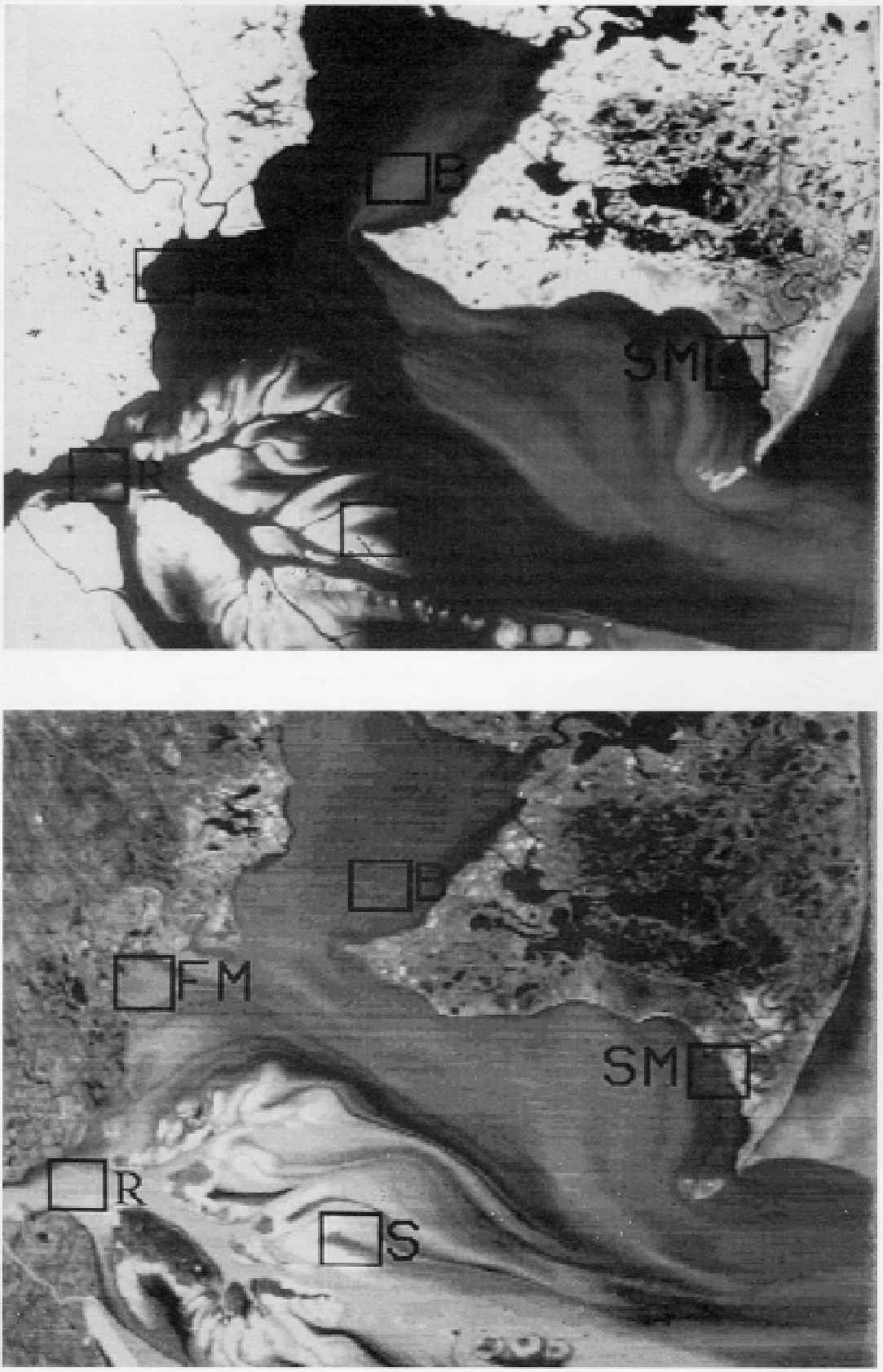

Figure 6. MAMS images of (a.) band 6 (0.65–0.83 μm) subsurface reflectance and (b.) split window surface temperatures for 5 December 1990, some 36 hrs after frontal passage. Boxes represent regions of images sampled for 6 December values shown in Figure 7. Note, although several water types are apparent on both days, there is a general reduction in contrast of water types from 4 December to 5 December, in tandem with a reduction in post-frontal winds and a rise in water level (as evidenced by partial submersion of deltaic deposits in the 5 December imagery.

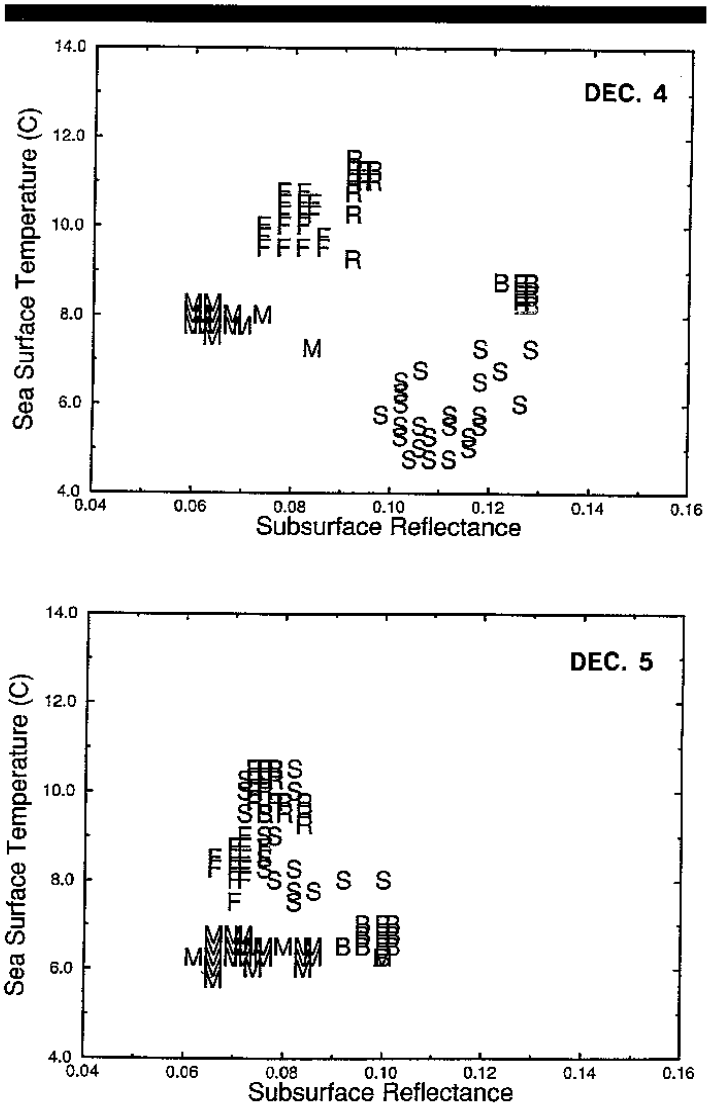

Figure 7. Scatter plots of MAMS remotely measured band 6 (.65–.83 μm) reflectance and split window SST for 4 December (top) and 5 December (bottom) 1990. Data sampled from labeled boxes in Figure 5: F = Fresh Marsh; B = Bay water; S = Soil water; M = Salt Marsh; R = River. Measurements of Gulf waters (not plotted) were 17 °C and 0.02 respectively. Note the clustering of measurements for each water type on 4 December. Some water types also apparent on 5 December, though groupings are more difficult to distinguish. Soil water on 5 December lacks true Soil water characteristics but is plotted as Soil water to demonstrate changing characteristics of colocated waters from 4 December to 5 December.

sediment concentration and SST measurements from a limited in situ data set collected on Dec 4, 1990. It is clear from Figure 7 that a bi-spectral approach aids in the separation of the water types. For example, the reflectance of bay water and soil water are similar; however the temperature signal of soil water clearly separates it from bay water. It should be pointed out that the "spread" of the soil water reflectances may in part be due to bottom reflectance in the very shallow water (< 1 meter) near the delta lobes (clear water penetration depth for channel 6 of approximately 1 m estimated from data provided in MOREL and PRIEUR (1977))

Water types plots for other MAMS visible and near infrared channels were produced and examined. Reflectance variation among water types was much reduced for the shorter wavelength radiation of channels 2 and 3 (blue/green region), and for channel 8, near infrared (channel 7 was not used due to sensor calibration uncertainty). Also channels 4 and 5 (orange/red) showed better differentiation between reflectances of river and fresh marsh waters than channel 6. These spectral dependencies are subjects of future study. The particular characteristics of these water types are dependent on the ambient conditions leading up to and at the time of observation. Seasonal variation in suspended material load and sea surface temperature will shift the plotted points in Figure 6 both left-right and up-down. We suspect that the relative position of each water type will be generally conserved through the cold front season. More observational data are necessary to test this idea.

ATMOSPHERIC FORCING, THE COLD FRONT CYCLE

During the cold front season (October–April), the subtropical U.S. Gulf Coast is repeatedly affected by the trailing edges of passing cold fronts, with mid-latitude cyclones typically tracking further north (PALMEN and NEWTON, 1969). Recent studies (ROBERTS *et al.*, 1987; HUH *et al.*, 1991) suggest that the annual series of cold front passages have as much or more long term impact on these environments than much rarer, but stronger hurricanes. Two important facts about cold-front passage events are: (1) the frequency of occurrence (30–40 yr^{-1}) and (2) the temporally and spatially ordered pattern of change in wind speed, direction, barometric pressure, temperature and humidity. It is important that the orientation of the cold front influences the wind direction, with fronts oriented normal (north-south) to the coast having a very different coastal wind field than those oriented parallel (east-west) to the coast (ROBERTS *et al.*, 1987).

The winter cold front cycle of temperate latitudes is a repeated sequence of events that imparts a burst of kinetic energy and an episode of rapid cooling to coastal and near shore shelf environments. A detailed study of a strong cold front passage and its impact on coastal waters was conducted by HUH *et al.* (1984). From it a simplified descriptive model of a cold front passage event is discussed in ROBERTS *et al.* (1987) and MOELLER *et al.* (1993). A practical consequence of a cold front passage is the regional dominance of a surface anticyclone within a few hours or days. The presence of the anticyclone optimizes optical and infrared remote sensing of the surface by typically bringing cool, dry, cloud-free air over the scene.

Cold front passages appear to play a significant role in the differentiation of water types. The pre-frontal rising sea level drives shelf waters over the shore face into coastal marshes and impedes river discharge into the Gulf. River water and sediment back up into the freshwater marshes and wetlands adjacent to the river channels. During the cold air outbreak phase, sea level set down induces seaward flow of the fresh and salt marsh waters that have been filtered of sediments by flowing through the marsh grasses. These low reflectance waters are routinely seen off Point Au Fer (salt marsh), Four

League Bay, East Cote Blanche Bay, and between the Wax Lake and Atchafalaya Deltas (Figures 1 and 3a). Water held in the sandy deltaic shoals is also released during sea level setdown. The presence of thin streamers of very cold waters from the Atchafalaya and Wax Lake Outlet deltas during mid-day warming was the first clue of this soil water drainage. Bay waters, responding to the cold front passage become colder and more turbid than the river waters, due to strong negative heat fluxes over broad shallow areas and bottom sediment resuspension.

Studies of images and scatter plots indicate that the various coastal waters form, evolve, flow, and generally dissipate in time. The few observations we have now through a cold front cycle indicate that after the initial burst of post-frontal atmospheric forcing, water types are differentiated to a maximum. As the post-frontal forcing weakens (hours to days after cold front passage), waters tend to homogenize. This is due to processes of cold front forced cooling and settling out of suspended sediments. This behavior is apparent in the water types analysis using MAMS data from 5 December 1990 (36 hours after the cold front passage) in Figure 7. Although the 5 December imagery (Figure 6) still shows good variability and indicates the presence of several water types, the plotted sample sites show how the water masses, especially marsh and soil water, have homogenized in both reflectance and temperature to the point that it is difficult to separate the types from one another. This suggests reduced marsh and soil water flow into the bay at the sample sites, a conclusion consistent with increased water levels in the bay. (Observations at New Orleans showed post-frontal winds had decreased to 2.6–5.1 m sec^{-1} from the northeast on 5 December, compared to about 7.7–10.2 m sec^{-1} from the north on 4 December, reducing the water level setdown forcing in the Atchafalaya Bay region.) The combination of reduced marsh and soil flow with the homogenization of water characteristics is probably responsible for the lack of separability in the 5 December plot. Instrumenting key outflow points around the Atchafalaya Bay region would further improve understanding of the impact of cold front passages on the cycle of marsh inundation and drainage, which is a key mechanism by which coastal marshes are supplied with invigorating sediments and nutrients.

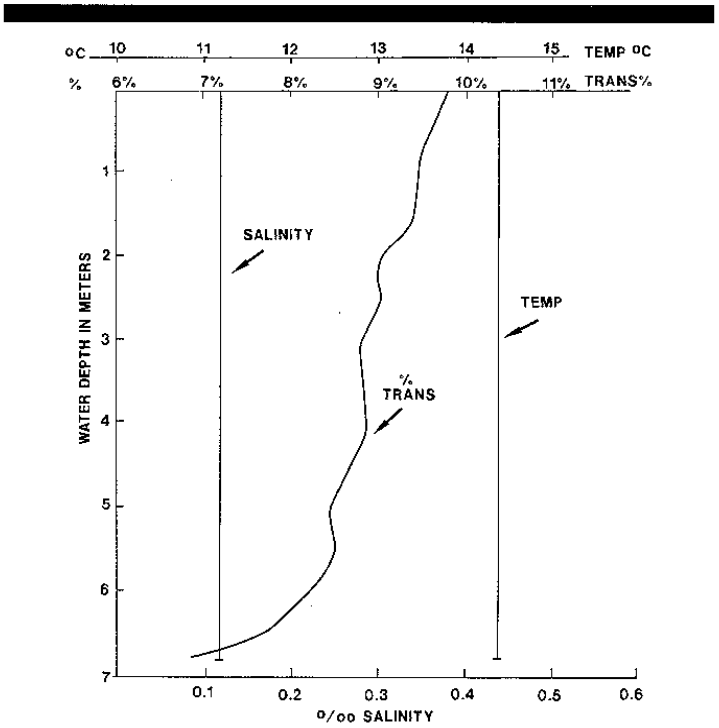

Figure 8. A temperature, salinity, and transparency profile obtained from a research vessel 24 hours after a cold front passage. The plot shows the destratified state of Atchafalaya River Discharge waters in the bay in terms of temperature and salinity with a subtle (3%) change in the transmittance (suspended sediment concentration) profile.

DISCUSSION

For coastal oceanographic applications, important questions are: (a) what is the physical significance of the temperature and reflectance measurements acquired by the MAMS and (b) how well can this instrument remotely measure them? The split window atmospheric correction algorithm allows a calculated estimate of water surface temperature which agrees with in-situ measurements to within 1 °C. However these MAMS radiometric thermal measurements originate from the top 1 mm of the water column. While this leaves the temperature structure of the bulk of the water column unsampled, it has been shown that during cold post-frontal conditions and under tidal stirring, shallow bay (<1 to 6 m depth) water temperatures are vertically well mixed (Figure 8). Thus, particularly under cold post-frontal conditions, one can assume that MAMS SST is representative of shallow bay water column temperature. This is not the case for suspended sediment load.

Reflectance of these coastal waters is controlled by seston content. In contrast to temperature, the reflectance measurements originate from varying levels depending on the scattering/absorption characteristics of the waters as a function of wavelength. For highly turbid bay or river discharge water, the signal originates from the top few decimeters (Figure 9) in most of the MAMS channels. In less turbid waters the signal originates from within the top meter (Figure 9). In shallow bay environments this can result in bottom reflectance being detected by the sensor. For this reason, it is advisable to choose spectral channels in the orange/red to near infrared range for reflectance measurements in bay or nearshore environments. The ambiguity imparted by detecting bottom reflectance possibly contributes to the reduction in reflectance range for the different water types observed in MAMS channels 2 and 3. In addition, vertical reflectance variation in the water column can be expected (see NANU and ROBERTSON, 1990) due to vertical gradients of suspended material. In the case of the Atchafalaya Bay region, vertical variation of water types is plausible as marsh, river, and soil waters drain into and override ambient bay waters. This also contributes to ambiguiety in reflectance observations from spectral channels that "see" further into the water column (*e.g.*, MAMS channels 2 and 3). These arguments suggest the combined use of orange/red - near infrared spectral data with thermal data for identifying water types.

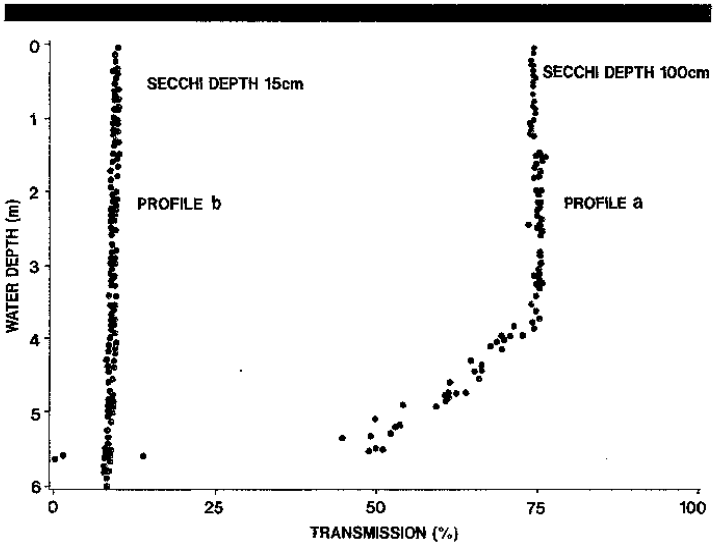

Figure 9. Water transparency profiles and secchi depth measurements in the Atchafalaya Bay before and after a cold front passage. These profiles show the distribution of light scattering particles (suspended sediments) in the water column, in two patterns, (a) pre-frontal pattern, a clear layer (75% transmittance) with a bottom turbid layer (50%–0% transmittance) of entrained sediment from before the frontal passage, and (b) post-frontal pattern, a highly turbid (8%), destratified completely mixed layer after the cold front passage.

Stratified water columns are the norm in the inner shelf seaward of the discharging deltas. The active river discharge plumes are seen to over-run waters of relict plumes (inactive and dissipating) that in turn are overriding warmer, more saline shelf waters. These flow westward with the prevailing coastal current, a flow interrupted by cold front passages that drive episodic eastward flow. The multiple ocean fronts are subjects of further studies.

CONCLUSIONS

Repeated coverage of coastal Louisiana with airborne and spaceborne high resolution multispectral scanner data combined with selective ground truth, is providing a powerful tool for coastal research and an important data base for environmental management. Understanding these complex environments has frustrated conventional data acquisition capabilities for many years. These data are providing an important historical record for analysis of long term changes in geomorphology and hydrology of these rapidly evolving Louisiana coastal-deltaic environments. This record is essential for development of environmental management programs important to sustaining and expanding the regional economy.

From the remotely sensed data and surface observations we recognize the following coastal water modification processes active in these environments:

(1) the rerouting of river discharge waters through fresh water coastal marshes by the damming effect of rising sea levels associated with the pre-frontal water level setup. Filtration of suspended sediment load from river waters by passage through grassy marshes renews marsh growth and reduces the reflectance of fresh marsh waters when they drain in post-frontal conditions,

(2) the flow of suspended sediment rich, inshore, marine waters through salt marsh areas, with subsequent filtering of sediment load reducing reflectance,

(3) the resuspension of bottom sediments in shallow waters of estuaries and river mouths, through cold front driven wave and current action, increasing bay water reflectance,

(4) the entrapment of river or estuarine waters as soil water within the sand banks of the newly formed deltas. These waters drain seaward under very low sea level stands associated with the cold air outbreak (post-frontal) phase of the cold front cycle. Low temperatures are results of the very short term exposure to solar warming, and

(5) the cooling or heating of standing, shallow surface waters by air-sea heat fluxes, heated or cooled dependant on atmospheric temperatures/humidity, wind speed, water depth, and time in the solar diurnal cycle.

These processes, individually or in combination are the primary generators of the multiple water types detected in the MAMS imagery. With the aid of cold front cycle forcings, these processes are put in motion culminating with an array of water types formed or released into the coastal environments in the post-frontal phase.

Study of these coastal waters through analysis of MAMS imagery reveals two important general facts:

(1) The best information content on these highly turbid (100–1200 mg l^{-1}) coastal waters is contained in the atmospherically corrected MAMS thermal infrared (sea surface temperature from band 11, 10.55–12.24 μm and band 12, 12.32–12.71 μm) and the orange/red-near infrared (MAMS channels 4–6, 0.57–0.67, 0.60–0.73, 0.65–0.83 μm respectively). The SPOT HRV-3 (0.79–0.89 μm) data also gives useful discrimination of water types (Figure 4b) at higher spatial resolution. Obtaining time series images of these data is important for studies of estuarine and coastal processes,

(2) the complex patterns of temperature and reflectance define repeatedly detectable coastal water types, whose source, areal extent, and evolution through time can be analyzed using sequences of this imagery. The MAMS data contains three basic kinds of information useful in identifying water types: temperature, reflectance, and aerial distribution patterns (*i.e.*, dimensions, orientation, boundaries, and associations). Utility of these tools are enhanced when applied in time-series to areally extensive, complex coastal processes.

Making meaningful and adequate measurements within the regional environment has been too costly or impossible with conventional methods. The advent of airborne and spaceborne sensor systems, global positioning systems, and rapid deployment boat operations provide for observations and measurements at the necessary time and space scales, and under conditions not previously possible.

ACKNOWLEDGEMENTS

The authors gratefully acknowledge support from Solid Earth Sciences Branch, Headquarters NASA, contract

NAGW-2052 at LSU and contract NAGW-3318 at University of Wisconsin, the former Office of Space Science and Applications, Headquarters NASA, contract NAGW-1745 at the University of Wisconsin–Madison, and U.S.G.S. project "Critical Processes of Wetland Loss", at L.S.U. Special appreciation is due the pilots and ground crews of NASA's ER-2 aircraft on deployment to the Gulf Coast from Ames Research Center (Moffett Field, CA) and to the Field Support Group of the Coastal Studies Institute for support of surface truth operations.

LITERATURE CITED

CRACKNELL, A.P., 1993. A method for the correction of sea surface temperatures derived from satellite thermal infrared data in an area of sunglint. *International Journal of Remote Sensing,* 14(1), 3–8.

GUMLEY, L.E.; MOELLER, C.C., and MENZEL, W.P., 1990. Monitoring of Mississippi delta coastal geomorphology using high resolution Multispectral Atmospheric Mapping Sensor (MAMS) data. *5th Australasian Remote Sensing Conference* (Perth, Australia), 738–745.

HUH, OSCAR K.; ROBERTS, HARRY H.; ROUSE, L.J., and RICKMAN, DOUG A., 1991. Fine Grained Sediment Transport and Deposition in the Atchafalaya and Chenier Plain Sedimentary System, *Coastal Sediments '91, Proceedings of Specialty Conference* (WR Divin in ASCE, Seattle, Washington, June), pp. 817–830.

HUH, OSCAR K.; ROUSE, LAWRENCE J. JR., and WALKER, NAN DELENE, 1984. Cold Air Outbreaks Over the Northwestern Florida Continental Shelf: Heat Flux Processes and Hydrographic Changes. *Journal of Geophysical Research,* 89(C1), 717–726.

JEDLOVEC, G.J.; BATSON, K.B.; ATKINSON, R.J.; MOELLER, C.C.; MENZEL, W.P., and JAMES, M.W., 1989. *Improved Capabilities of the Multispectral Atmospheric Mapping Sensor (MAMS).* NASA Technical Memorandum 100352, Marshall Space Flight Center, Huntsville, Alabama, 71p.

KLEMAS, V., 1980. Remote sensing of coastal fronts and their effects on oil dispersion. *International Journal Remote Sensing,* 1, 11–28.

MOELLER, CHRISTOPHER C.; HUH, OSCAR K.; ROBERTS, HARRY H.; GUMLEY, LIAM E., and MENZEL, W. PAUL, 1993. Response of Louisiana Coastal Environments to a Cold Front Passag. *Journal of Coastal Research,* 9(2), 434–447.

MOELLER, CHRISTOPHER C.; GUMLEY, L.E.; MENZEL, W.P., and STRABALA, K.I., 1989. High resolution depiction of sea surface temperature and suspended sediment concentrations from MAMS data. *Proceedings, Fourth Conference on Satellite Meteorology and Oceanography* (American Meteorological Soc. Boston, pp. 208–212.

MOREL, A. and PRIEUR, L., 1977. Analysis of variations in ocean color. *Limnological Oceanography,* 22, 709–722.

NANU, L. and ROBERTSON, C., 1990. The effect of suspended sediment depth distribution on coastal water spectral reflectance: Theoretical simulation. *International Journal of Remote Sensing,* 14(2), 225–239.

PALMEN, E. and NEWTON, C.W., 1969. *Atmospheric Circulation Systems.* New York: Academic, 603p.

PENLAND, SHEA and RAMSEY, KAREN E., 1990. Relative Sea-Level Rise in Louisiana and the Gulf of Mexico: 1908–1988. *Journal of Coastal Research,* 6(2), 323–342.

REED, D.J., 1989. Patterns of sediment deposition in subsiding coastal salt marshes, Terrebonne Bay, Louisiana: The role of winter storms. *Estuaries,* 12(4), 222–227.

ROBERTS, H.H.; HUH, O.K.; HSU, S.A.; ROUSE, L.J. JR., and RICKMAN, D., 1987. Impact of cold-front passages on geomorphic evolution and sediment dynamics of the complex Louisiana Coast. *Coastal Sediments '87.* (WW Div./ASCE, New Orleans, Louisiana, May 12–14, 1987), pp. 1950–1963.

ROBERTS, H.H. and VAN HEERDEN, I., 1992. *Atchafalaya-Wax Lake Delta Complex, the New Mississippi River Delta Lobe.* Coastal Studies Institute Industrial Associates Report, Baton Rouge, Louisiana, 78p.

STUMPF, R.P., 1983. The processes of sedimentation on the surface of a salt marsh. *Estuarine, Coastal and Shelf Science,* 17, 495–508.

SUOMI, V.E.; FOX, R.; LIMAYE, S.S., and SMITH, W.L., 1983. McIDAS III: A modern interactive data access and analysis system. *Journal of Climate and Applied Meteorology,* 22, 765–778.

WALKER, NAN D. and ROUSE, LAWRENCE J. JR., 1993. *Satellite Assessment of Mississippi River Discharge Plume Variability.* Minerals Management Service Report prepared under Interagency Agreement 14-35-0001-30470, 46p.

WANG, FLORA C.; LU, TIESONG, and SKORA, WALTER B., 1993. Intertidal Marsh Suspended Sediment Transport Processes, Terrebonne Bay, Louisiana, U.S.A. *Journal of Coastal Research,* 9(1), 209–220.

WEN-YAO; FIELD, L.R.; GANTT, R., and KLEMAS, V., 1987. Measurement of the surface emissivity of turbid waters. *Remote Sensing of Environment,* 21, 97–109.